Analysis and Modeling of Burr Formation During the Plane Milling of Cast Aluminum Alloy Using Polycrystalline Diamond Tools

Clément Bourlet
Arts et Metiers ParisTech,
LaBoMaP,
Rue Porte de Paris,
Cluny 71250, France

Guillaume Fromentin
Arts et Metiers ParisTech,
LaBoMaP,
Rue Porte de Paris,
Cluny 71250, France

Elias Harika
Montupet,
3 Rue de Nogent,
Laigneville 60290, France

Arnaud Crolet
Montupet,
3 Rue de Nogent,
Laigneville 60290, France

Burr formation is a significant problem during manufacturing and leads to a lack of geometrical quality through the appearance of undesired and undefined shapes on the workpiece. Thus, understanding the burr formation and elaborating of predictive models are helpful for process design in order to avoid or to reduce burrs and to optimize the strategies for eventual deburring. This study presents both an experimental approach and a model for the plane milling of openwork parts, where burrs are a significant factor. A large-scale analysis of relevant geometrical parameters and their interactions are performed. A phenomenological burr size model is established considering local parameters and the specificities of 3D cutting in milling. Based on local parameters, this article proposes a new methodology to simulate burr height along any part edge and for most face-milling trajectories. Simulations and validations during tool path exits, with changing local parameters, are presented. In addition to the quantitative approach, new 3D aspects of face milling in relation with exit order sequence (EOS) are developed.

1 Introduction

Quality is an increasingly important requirement in parts machining. Meanwhile, burrs may appear in various cases of machining operations [1] and become highly problematic when producing parts made of ductile alloys. Machining strategies have to reduce burr formation, or at least their appearance must be predictable in order to define deburring solutions during the design of the manufacturing process. As a consequence, various scientific works have been developed concerning burrs, as regards their physical understanding, control, and removal [1].

It is established that there are various mechanisms which induce burrs. They may lead to Poisson burr, tear burr, or rollover burr [2], and the burr type is fundamentally linked to the geometrical configuration of the cutting process and to the workpiece material properties (ductile or brittle).

Most modeling investigations are focused on rollover burr formation. These are also called exit burrs and are formed at the end of the cut due to a large plastic deformation, which creates a pivoting point at the chip root linked to the workpiece [3] in the case of ductile alloys. This fundamental burr formation process was recently observed using a high-speed camera [4]. Several approaches have been developed to study the basic understanding of exit burr formation in orthogonal cutting. Analytical models of the burr thickness linked to rollover burr formation resulting from plastic shear deformation have been established [2,5]. If the chip fracture does not appear, depending on the strain hardening and fracture behaviors of the workmaterial, these analytical approaches also allow for the evaluation of the burr height. The use of a finite-element method (FEM) [4,6–8] results in a more precise evaluation of the burr formation; nevertheless, it needs adequate constructive law, friction, and damage models of the workmaterial. Although these studies generate an important understanding and allow for the evaluation of parameter effects, the burr formation is significantly affected by the geometrical configuration of the cutting process, and orthogonal cutting differs a lot from a milling operation using a tool with a nose.

During flank or slot milling, side burrs as well as bottom burrs may appear and their sizes will especially depend on the following geometrical parameters: tooth exit angle (i.e., cutting speed direction versus workpiece border) and workpiece wedge angle. This 3D geometrical aspect constitutes a major difference between the orthogonal cutting and the milling process.

Nonetheless, analytical modeling on burr formation in slot milling of ductile materials has been developed [9,10]. These works are based on the burr formation model established for orthogonal cutting [5] coupled with a mechanistic force model. This approach can predict the side burr thickness, but unfortunately not the bottom burr height which is the main requirement in plane milling.

Both the bottom and the side burr formation have been simulated from a complete 3D FEM in milling [8]. In addition to the difficulties in orthogonal cutting, the computation of a 3D cutting process is complex and requires a long time. As a consequence, the authors proposed a methodology to approximate the 3D milling process with orthogonal cutting in the chip flow plane, which is not an appropriate assumption for determining the bottom burr as well as for analyzing the effect of the 3D geometrical configuration.

Many experimental studies have been conducted on bottom burr formation during face milling, mostly in ductile alloys: aluminum alloy [8,11,12], stainless steel [3,13,14], carbon steel [15,16], and gray cast iron [17]. It has been demonstrated that several parameters clearly affect burr formation, such as cutting edge geometry (rake angle and nose geometry), tool wear, tooth exit angle, or radial and axial depth of cut, feed, and cutting speed [8,11–17]. Not all the studies have analyzed the interaction between feed and radial depth of cut, which nevertheless affects the uncut chip thickness. In addition, the analyses are usually focused on exit lateral burrs generated with constant influential parameters, i.e., not on bottom burr.

From most of these investigations, the tooth exit angle appears to be a major parameter in bottom burr formation. Moreover, it is
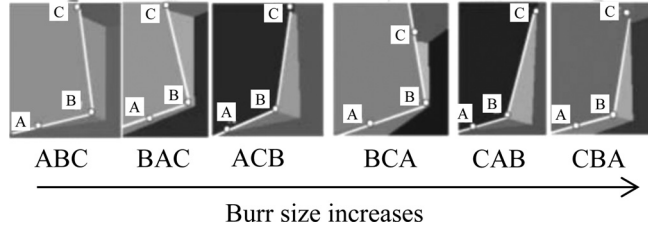
ABC   BAC   ACB   BCA   CAB   CBA

Burr size increases

Fig. 1   Effect of EOS on bottom burr size [18]

established that the EOS of the cutting edge along the workpiece edge is also a preeminent criterion [3,18], cf. Fig. 1. Based on all these geometrical considerations, the milling tool path can be adapted in order to avoid or minimize burr formation [19].

Nonetheless, the EOS has been developed with a restriction on the workpiece wedge angle equal to 90 deg. Unfortunately, neither EOS consideration nor 3D FE modeling has been used in a unified analysis including different tooth exit angles and different workpiece wedge angles. This analysis is necessary for better understanding the interaction between side burr and bottom burr formation, as explained in Ref. [3]. This interaction is mainly related to the instantaneous engagement of both minor and major cutting edges, and consequently, to the strength of the chip root in both directions. The physical explanation behind the EOS approach could mainly be related to this interaction.

In summary, the literature review shows very few studies dealing with the modeling of bottom burr formation in milling and most are focused on experimental analyses of burr height generated in constant conditions. Furthermore, all the 3D geometrical specificities of the milling process are not widely taken into account.

This article focuses on the burr formation during the plane milling of cast aluminum alloy using polycrystalline diamond (PCD) tools, such as cylinder head machining in the automotive industry. In this case, the geometrical conditions affecting the bottom burr size vary considerably because of the openwork parts.

The aim of this study is to propose a method to analyze milling conditions, combined with an experimental approach to establish a burr size model based on local geometrical parameters. Thus, the cutting exit angle, workpiece edge orientation, and workpiece wedge angle are considered. From this phenomenological model and the geometrical approach, with considerations for local geometrical conditions, this study provides a new method to determine and quantify the burrs resulting from plane milling on any edge of an openwork part. In such case, influent local parameters on burr height are inconstant. Simulations and experimental validations are presented.

2   Approach of the Study

The objective is to develop a generalized quantitative approach for burr formation in plane milling, whether a face-milling path or several end-milling paths are used.

The term "face-milling" will be used to define a milling configuration with no shoulder, i.e., the radial depth of cut is equal to the workpiece width. In this milling configuration, two main bottom burr types may appear, as shown in Fig. 2: entry burr and exit burr.

The term "entry burr" (respectively, "exit burr") designates here the burrs obtained when the teeth are entering the workmaterial (respectively, going out from the material). These terms were used by other authors to designate the burrs obtained when the tool is entering or going out from the piece, which is not appropriate for our approach based on local geometry. Indeed, at a given position of the tool (tool entrance or tool exit), teeth are entering and going out from the piece at the same time. The burrs obtained in the region of the teeth exit are usually greater and this study

mainly focuses on them. A deeper study of entry burrs will be the purpose of the next work.

The term "end-milling" will be used to designate a milling configuration with a small shoulder. In this milling case, other burr types may appear, such as side and top burrs. Our investigations are not focused on them, because they will be removed by the next end-milling paths applied to generate a complete workpiece plane.

Therefore, this study deals with "exit bottom burrs" considering that both face milling and end milling can generate them (the main difference is related to the presence of material on the lateral shoulder).

During milling, the cutting parameters on workpiece lateral edges are constant when the feed direction is parallel to the edge ($\psi = 0$ deg or $\psi = 180$ deg according to Fig. 2). When they are not parallel, the cut thickness and the cutting direction change continuously along the edge. Consequently, burr formation will be quantified along the lateral exit edge, and a local geometrical approach is developed below to predict burr height in any milling configuration using local parameters defined further down.

The tool used is an 80 mm diameter and nine teeth face-milling cutter supplied by Ceratizit. Two PCD cutting insert geometries are tested: rounded-nose and chamfered-nose insert. The cutting geometry of the milling cutter is detailed in Fig. 3. The milling cutter is used with only three PCD inserts to reduce their consumption. It is assumed that locally, teeth trajectories through the boundaries of the part would be the same as when the mill is equipped with nine inserts, as well for the results of the study in terms of burr size. Investigations are performed for the milling of AlSi7Mg0.3Cu0.5 cast aluminum alloy with a coolant.

2.1   Geometrical Parameterization. For a milling configuration, it is assumed that only local parameters may be responsible for burr formation when cutting material on the workpiece boundaries. As a consequence, the following parameters are defined in Fig. 4:

- the workpiece wedge angle, Δ, which has not been studied until now,
- the uncut chip thickness at the cutting edge exit, h_{ex}, which results from the feed and the radial depth of cut,
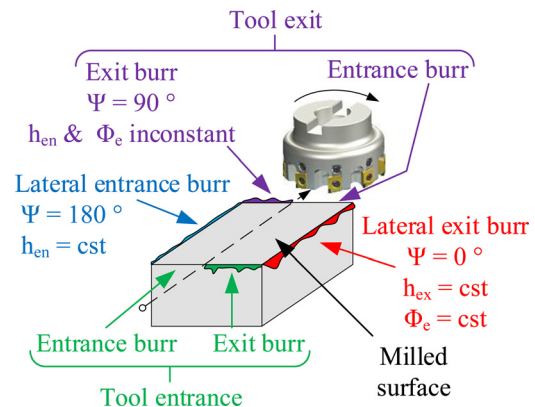

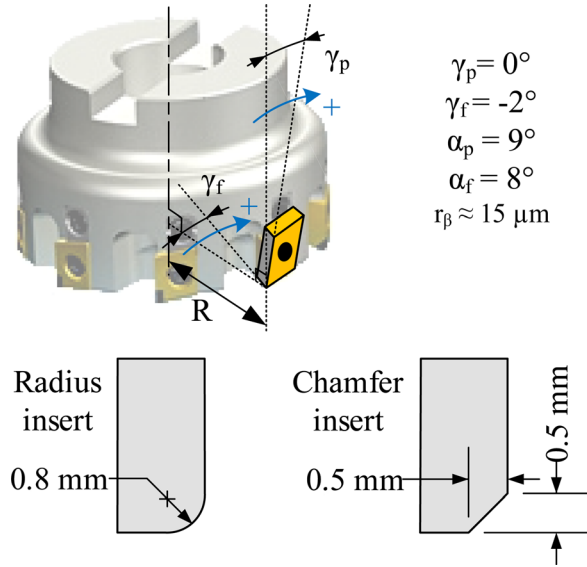**Fig. 2   Bottom burr types during face milling**

$\gamma_p = 0°$
$\gamma_f = -2°$
$\alpha_p = 9°$
$\alpha_f = 8°$
$r_\beta \approx 15\ \mu m$

Fig. 3 Milling cutter and insert characteristics

- the cutting edge exit angle, ϕ_e, which depends on the radial depth of cut and on the workpiece edge orientation Ψ versus the feed direction, cf. Fig. 2.

In the case of exit burrs, the cutting edge exit angle ϕ_e varies between -90 deg and $+90$ deg and is equal to 0 deg when the cutting direction is collinear with the normal direction of the workpiece boundary. It means the closer to 0 deg this angle is, the higher the cutting force acting on the workpiece, i.e., in the direction of the burr formation. Moreover, the cutting force intensity is linked to the cut area, i.e., to the uncut chip thickness h_{ex} and to the axial depth of cut a_p.

It is worth noting that plane milling operations can be achieved using different strategies: one face-milling tool path or several end-milling tool paths. Furthermore, two main configurations can appear.

When the feed direction is parallel to the workpiece edge ($\psi = 0$ deg or $\psi = 180$ deg), the cutting edge exit angle ϕ_e and the
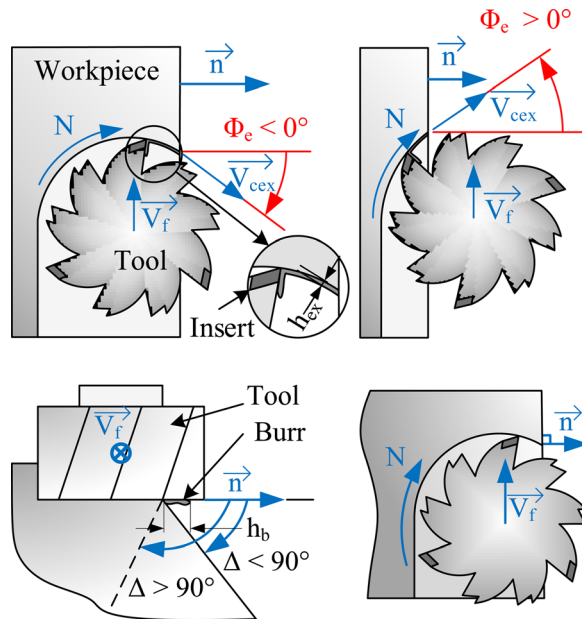
uncut chip thickness at the cutting edge exit h_{ex} can be evaluated as presented in Appendix A.

When the two directions are not parallel, there are three states during a milling penetration or exit. Appendices B and C present these steps and the ϕ_e and h_{ex} determination during milling exit and entry, respectively. Furthermore, the radial depth of cut value has to be considered to limit the value of angular parameters.

2.2 Experimental Procedure and Burr Characterization. The burrs are analyzed using two different devices. A high-definition camera is used to observe the burr, face-on to the milled plane, cf. Fig. 5. Mainly, wave exit burrs are generated during milling. The measurement methodology then allows to characterize the burr height variation and the burr type. Using this method, it is not possible to measure the absolute burr height, because the workpiece lateral face is hidden by the burr.

Second, burr heights are measured in various cross sections with a mechanical scanning device as shown in Fig. 6. The device precision is lower than $0.5\ \mu m$. The burr height is determined from the maximum height during one profile measurement. Twenty profile measurements, separated by 0.2 mm, are performed to locally characterize the burr in one zone. Then, three sets of 20 profile measurements are carried out to characterize the burr at different locations along a workpiece boundary resulting from one milling test. From these data, statistical analyses are performed, and the average burr height $h_{b\ ave}$ and the maximum burr height $h_{b\ max}$ are determined.

3 Experimental Results and Analysis

3.1 Preliminary Results. The conducted trials demonstrate that varying the cutting speed between 1500 m/min and 4500 m/min has no effect on burr height, whereas a slightly increasing effect in a different context was observed during aluminum milling [11] and a decreasing one during medium carbon milling [15]. Other preliminary investigations were carried out in order to identify the parameters having a significant effect on burr formation, before executing complete analyses limited to these parameters and considering their interactions. Preliminary results are summed up below.

3.1.1 Burr Types. It can be seen in Fig. 5 that no lateral burr, either positive or negative, is generated at the workpiece boundary face onto the teeth entry. The workpiece edge sharpness is so good that no burr height is measured. It may be different with a worn tool, but this is presently not studied.

As mentioned previously, wave exit burrs are obtained after milling. Most of these are burr type 9 (exit bottom burr) as defined
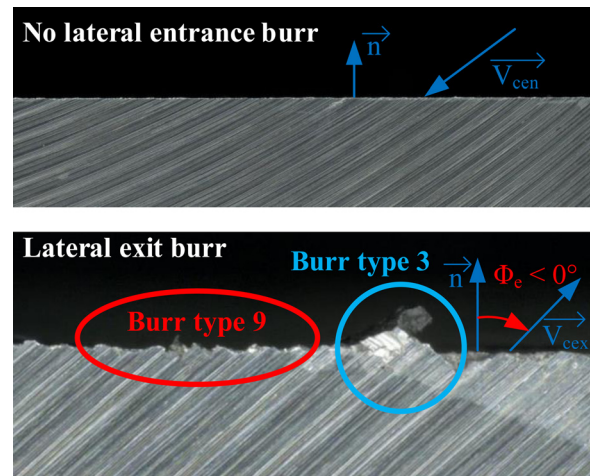

Fig. 4 Geometrical and kinematic parameters definition in end milling

Fig. 5 Observations of burr type and entry/exit effect in full face milling
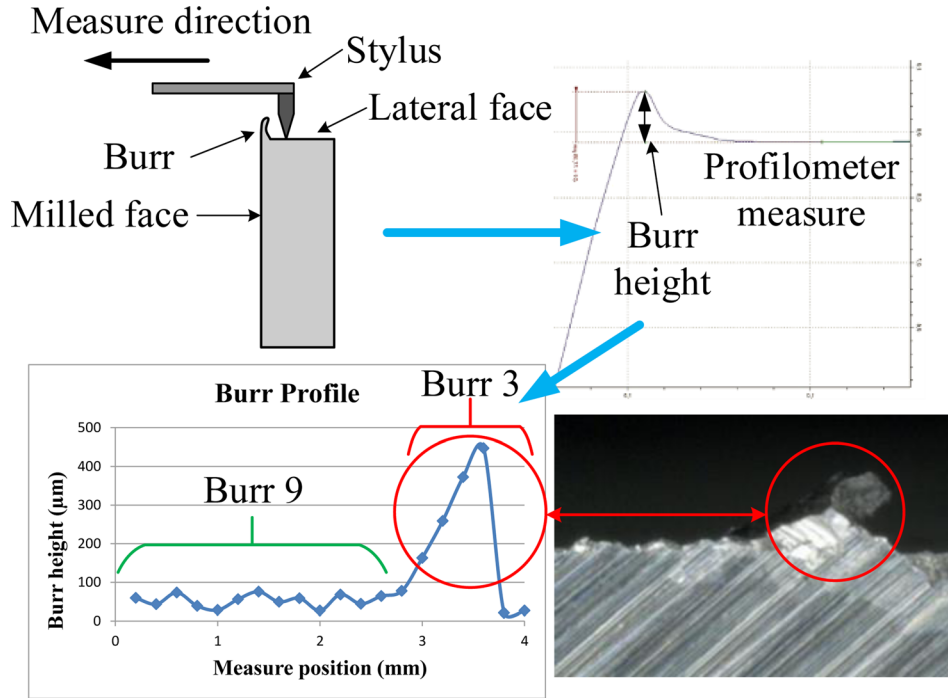
Fig. 6 Burr height measurement methodology with mechanical profilometer

in Refs. [14–16]. However, higher burrs may occasionally appear, but they can be very easily removed as soon as they are slightly pushed. These observations match with primary burr and secondary burr mentioned in Refs. [3] and [15]. Their size seems to be correlated to the axial depth of cut. Consequently, it is supposed that these burrs are ultimately side burrs, burr type 3 (exit up milling side burr), generated by the major cutting edge and very weakly linked to the workpiece. Because they are easily removed, burrs of this type are not quantified and not taken into account in h_b criteria (average and maximum) in all the quantitative results presented, neither for the burr model determination.

3.1.2 Cumulative Effect of Burr Formation. In flank milling, a phenomenon of increasing exit bottom or side burrs may appear after each cut and lead to a significant burr height. Several sets of face-milling tests are conducted on the same sample, by engaging the tool each time on the previously machined surface. The intention is to establish whether the exit burr becomes higher after each milling path or it remains the same.

The tested depths of cut are 0.15 mm, 0.5 mm, and 3 mm. A constant exit side burr height is observed after each tool path; thus, no increase appears. This can be explained by the fact that the burr thickness would still be inferior to the depth of cut. There is no need to investigate a lower depth of cut, because finish milling is applied with a higher value than 0.15 mm.

If a cumulative effect had existed, then the initial surface preparation might have affected all the parameter investigations.

3.1.3 Cutting Geometry Effect. Two different cutting geometries are tested: rounded nose and chamfered nose. Their effect on average burr height depends on the depth of cut. For a value of 0.15 mm, when the tool noses are slightly engaged and the lead angle oriented through the milling surface, the average burr height is 46 μm with the rounded nose and 51 μm with the chamfered nose. This demonstrates that the rounded nose slightly reduces the type 9 burr height.

These results can be geometrically and mechanically explained by the resultant acting force or the chip flow direction [15,16] and as function of the depth of cut.

Nevertheless, the experiments also show that milling with rounded-nose inserts leads to the appearance of a large number of

type 3 burrs. For this reason, the chamfered-nose inserts are used for the rest of this study.

3.2 Extended Investigations

3.2.1 Depth of Cut Effect. The axial depth of cut is a parameter which is generally studied, because it particularly affects exit burr formation. Figure 7(a) shows that a higher depth of cut increases the burr height, but not linearly from 0.15 to 3 mm. Furthermore, these results demonstrate the significant variation in burr height, the maximum value being more than twice the average one. Figure 7(b) shows the burr height distributions. They are nonsymmetrical and there are more burrs having a height greater than the mean than those having a lower one.

The cellular dendritic structure of the workmaterial is around 1 mm, whereas the distance between two measured profiles to determine the burr height is equal to 0.2 mm. Thus, a cause of burr height variation may be the structural heterogeneity of the material. No complementary investigations were performed with respect to this burr height variation.

3.2.2 Exit Angle Effect. The cutting edge exit angle greatly influences the direction of the workmaterial flow and the cutting force and thus modifies the burr formation. Analyses were performed considering symmetrical values for the ϕ_e angle, as shown in Fig. 8. During these tests, the feed was always constant; thus, the change in the radial depth of cut also gives rise to different values for the h_{ex} uncut chip thickness at the cutting edge exit. Nevertheless, the h_{ex} values are the same for symmetrical configurations.

These experiments show a combined effect of ϕ_e exit angle and h_{ex} uncut chip thickness on the burr height. Furthermore, they also prove that there is a trend toward a decrease in burr height when changing from a negative ϕ_e exit angle (with $a_e > R$) to a positive one (with $a_e < R$), h_{ex} being constant between symmetrical values.

This observation can be made regarding other investigations on the EOS of the cutting edge [3,18]. In the present study, the radial rake angle is negative, and the axial rake angle is zero, so the B and C points exit at the same time when the workpiece wedge angle Δ is equal to 90 deg. Thus, if the radial depth is lower to the tool radius, the EOS is A → (BC), whereas it is (BC) → A when

(a)

(b)
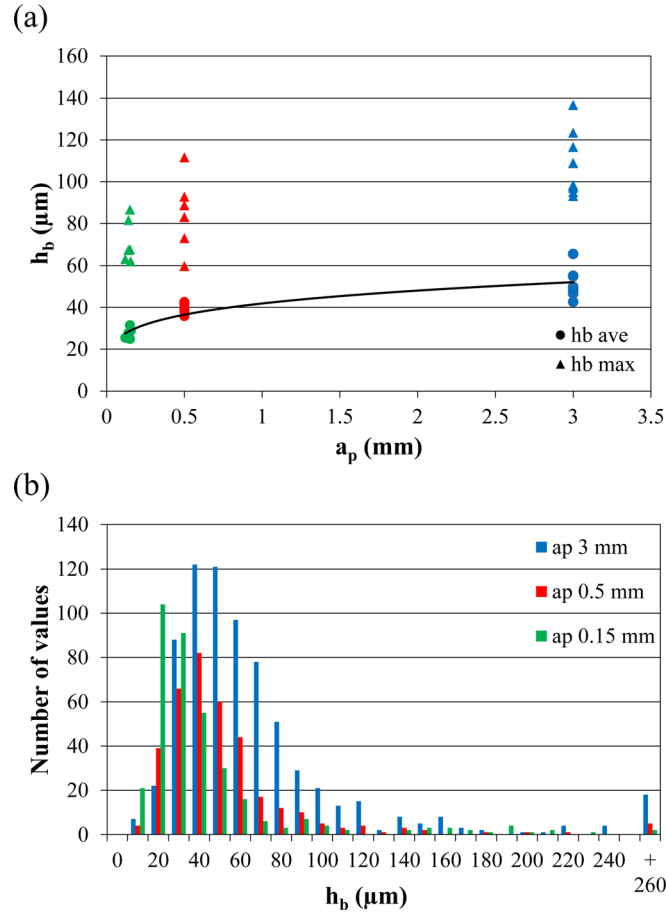
Fig. 7 Effect of the depth of cut on burr height: $V_c = 2500$ m/min, $f_z = 0.25$ mm $\cdot$ rev$^{-1}\cdot$th^{-1}, $\Phi_e = -48.6$ deg, and $\Delta = 90$ deg

the radial depth is larger. It is established from the geometrical analyses and confirmed by the experimental results [3,18] that the first EOS is more favorable for reducing the burr formation.

It should be noted that the burr formation results from a 3D geometrical configuration. The geometrical analysis defining the EOS is a qualitative 3D approach. From the geometrical approach used in the present article, direct 2D quantitative criteria are defined, but it is shown that the sign of the exit angle ϕ_e is sensitive to the 3D aspect.

3.2.3 Workpiece Wedge Angle Effect. Fundamental studies on the burr formation in orthogonal cutting have dealt with the effect of the exit angle. When considering a 3D problem such as face milling, the workpiece wedge angle is a second angle to take into account, in the direction of the minor cutting edge. This angle is in direct relation to the part design.

EOS is considered as a qualitative criterion which is useful for burr formation prediction, and a quantitative correlation has been made between EOS and burr height [18]. As a consequence, in
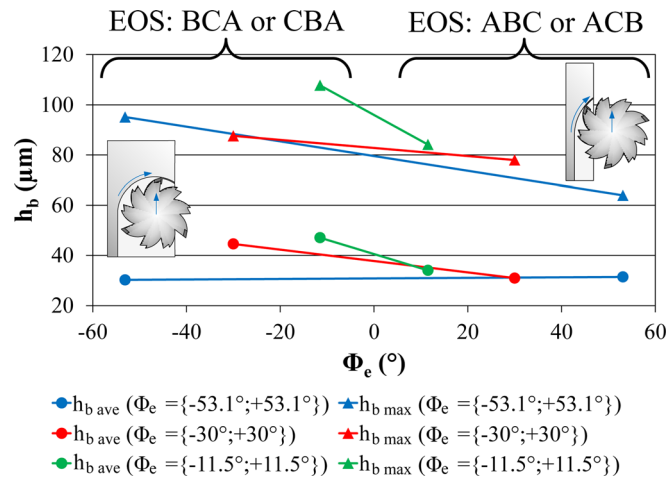

Fig. 8 Effect of opposite cutting edge exit angle on burr height: $V_c = 2500$ m/min, $f_z = 0.25$ mm.rev^{-1}.th^{-1}, $a_p = 1$ mm, and $\Delta = 90$ deg

addition to the previous work [3], an extended geometrical approach to EOS is developed in order to take into account the workpiece wedge angle Δ. It is presented in Fig. 9.

A study of the workpiece wedge angle effect should require the preparation of a set of workpieces having different angle values. In order to avoid having to produce these, a different strategy is used. A basic sample with a groove having circular cross section (generated with a ball-end mill) is prepared. As shown in Fig. 10, the orientation of the tangent to the groove at the milled surface changes from 90 deg to 0 deg, after milling using one tool with a given depth of cut. Furthermore, the groove geometry is defined to keep the radial depth of cut constant. Thanks to this experimental setup, it is possible to investigate the workpiece wedge angle effect in the range from 0 deg to 90 deg over a single tool path. For higher values, it is necessary to proceed differently with a new workpiece having a differently oriented groove.

Figure 11 presents the effect of the wedge angle from 40 deg to 160 deg. The exit burr height was not measured in accordance with ISO 13715 standard [20], because we consider that it has more physical meaning to measure the burr height in its flow direction, and that this is more appropriate for the modeling approach. The effect of the wedge angle is significant, and the burr height increases quite linearly with the wedge angle. A lower wedge angle, for instance 40 deg, induces a burr height limited to 10 μm, which is easily understandable geometrically. The wedge

Fig. 10 Workpiece geometry to study the effect of the wedge angle

angle is defined in the cross section of the burr flow, and the wedge locally affects the strength of the chip bottom root and thus burr formation.

When analyzing these results with an EOS approach, we find that even if the axial rake angle is null, when the wedge angle is different from 90 deg, points B and C do not exit at the same time from the material. These results demonstrate, although all the other cutting conditions are constant, that an ABC EOS may generate a higher burr height than the CAB one. This EOS ranking differs from the one previously established in Ref. [18], cf. Fig. 1 with Δ = 90 deg. Therefore, it is necessary to consider that the relation of EOS ranking versus burr height is affected by the workpiece wedge angle. Indeed, when the workpiece edge is wedged (Δ < 90 deg), the chip bottom root is strong enough for the cutting process and the interaction with the lateral material begins trivial. Finally, the validity of one EOS ranking would have to be established as a function of a given set of conditions, among the workpiece wedge angle.

4 Modeling

Based on the previous investigations, a design of experiment (DOE) approach is proposed to quantify not only the parameter effect but also their interactions. From this, a local model of the burr height is determined. The use of this model for the plane milling of a complete part is supported by the geometrical model. This evaluation could not be done with the EOS approach alone because the burr height is not constant for a fixed EOS and it depends on the other studied parameters.

Fig. 9 EOS determination considering workpiece wedge angle Δ

Fig. 11 Effect of workpiece wedge angle on burrs height: V_c = 2500 m/min, f_z = 0.25 mm.rev^{-1}.th^{-1}, a_p = 1 mm, and Φ_e = 0 deg

Table 1 Experimental tests and DOE matrix

| Tests | Standardized variables | | | Local variables | | | | Global variables | | Results |
	h_{ex}^*	ϕ_e^*	a_p^*	h_{ex} (mm)	ϕ_e (deg)	a_p (mm)	Δ (deg)	f_z (mm.rev^{-1}.th^{-1})	a_e (mm)	$h_{b\ ave}$ (μm)
1	−1	−1	−0.06	0.05	−48.6	1	{46, 67, 90}	0.076	70	{35, 49, 69}
2	+1	−1	−0.06	0.2	−48.6	1	{46, 67, 90}	0.302	70	{29, 38, 50}
3	−1	+1	−0.06	0.05	0	1	{46, 67, 90}	0.05	40	{35, 47, 48}
4	+1	+1	−0.06	0.2	0	1	{46, 67, 90}	0.2	40	{44, 57, 60}
5	−1	0	−0.96	0.05	−25.2	0.15	{46, 67, 90}	0.55	57	{29, 34, 34}
6	−1	0	+1.03	0.05	−25.2	2	{46, 67, 90}	0.55	57	{33, 43, 44}
7	+1	0	−0.96	0.2	−25.2	0.15	{46, 67, 90}	0.221	57	{33, 44, 48}
8	+1	0	+1.03	0.2	−25.2	2	{46, 67, 90}	0.221	57	{39, 55, 70}
9	0	−1	−0.96	0.125	−48.6	0.15	{46, 67, 90}	0.189	70	{36, 48, 63}
10	0	+1	−0.96	0.125	0	0.15	{46, 67, 90}	0.125	40	{35, 45, 59}
11	0	−1	+1.03	0.125	−48.6	2	{46, 67, 90}	0.189	70	{40, 56, 85}
12	0	+1	+1.03	0.125	0	2	{46, 67, 90}	0.125	40	{47, 62, 67}
13	0	0	−0.06	0.125	−25.2	1	{46, 67, 90}	0.138	57	{42, 54, 61}

4.1 Local Model of Burr Height. The applied DOE approach is restricted to the following parameters, which show significant effects during preliminary investigations: h_{ex}, ϕ_e, Δ, and a_p. The parameter values are mentioned in Table 1, resulting in 13×3 tests. The feed and the radial depth of cut are defined in order to set independently the values of the exit angle ϕ_e and the uncut chip thickness h_{ex}. This is necessary in order to evaluate the effects separately from the interactions.

Further, the study being focused on face milling, only negative values of exit angle ϕ_e are investigated, i.e., $a_e \geq R$, which generate slightly higher burr than in the opposite configuration, according to the previous result.

Figure 12 presents the effect and the interaction of the parameters on burr height. It appears that the highest effects are those pertaining to the wedge angle and the depth of cut. The physical understanding of these parameter effects is already discussed in Sec. 3.

The next most important effect is the interaction between the exit angle ϕ_e and the uncut chip thickness h_{ex}. The independent effects of these two parameters are not significant when considering a 95% value for the Fischer test. Nevertheless, uncut chip thickness h_{ex} is worth taking into account. The effect of exit angle ϕ_e by itself does not exist.

Leaving to one side the exit angle ϕ_e effect, the next influential parameters with respect to burr height are second- and third-order interactions; the following ones depend on the workpiece wedge angle.

From all these experimental results, correlation analyses between the burr height and the EOS are performed by selecting 1–6 from the six possible sequences. When considering all the tests, the correlation coefficient is around 43%, which does not allow us to conclude that the EOS ranking fits with the burr height in any conditions. This poor correlation proves one more time the nonvalidity of the former EOS ranking when $\Delta \neq 90$ deg. Further analysis of this correlation would be justified only if the field of investigation had included the six possible EOS. Nonetheless, it seems that this correlation and EOS ranking versus the burr height could be linked to a parameter domain and may depend on the wedge angle.

Concerning burr height modeling, an effect and interaction additive model, usually established in a DOE approach, would give non-null values even if the h_{ex} thickness were null. Consequently, a more realistic phenomenological local model of the burr height is formulated, as in Eq. (1). Let us consider the first term, which can be associated with the force toward the normal direction to the workpiece edge and which is responsible for the burr formation. Thus, for h_{ex} and ϕ_e equal to zero and 90 deg, respectively, the burr height is null. The second term integrates a dissociated effect of the depth of cut and the workpiece wedge angle. This model is identified with a least mean square method,

from the tests presented in Table 1; the average relative error is only 12% and the maximum is 33%. Without taking into account the five worst tests (i.e., the other 34 tests are considered), the maximum relative error is equal to 23%. Thus, the model precision is quite acceptable, especially since the burr height is rather variable

$$h_b = (h_{ex} \cdot \cos \phi_e)^{k_1} (k_2 + k_3 \cdot a_p{}^{k_4} + k_5 \cdot \Delta^{k_6}) \quad (1)$$

4.2 Global Model for Plane Milling. This section deals with a real case of tool exit during face milling. The approach could also be applied for the tool entry, and further, for any value of the angle Ψ. Thus, based on the phenomenological local model, and on geometrical considerations, burr height distributions along a workpiece edge during a tool path exit are studied.

Three configurations with different workpiece edge orientations Ψ: 60 deg, 90 deg, and 120 deg are considered. Appendix B is used and the analysis is performed with a radial depth of cut equal to the tool diameter, which finally enables us to consider every
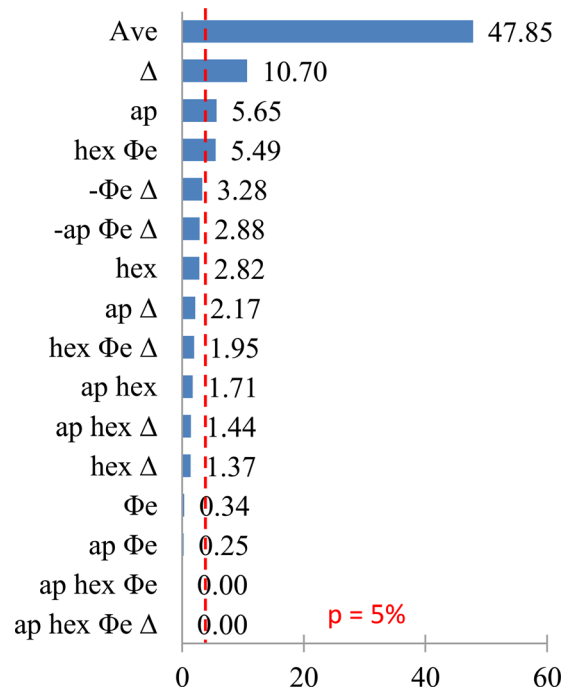

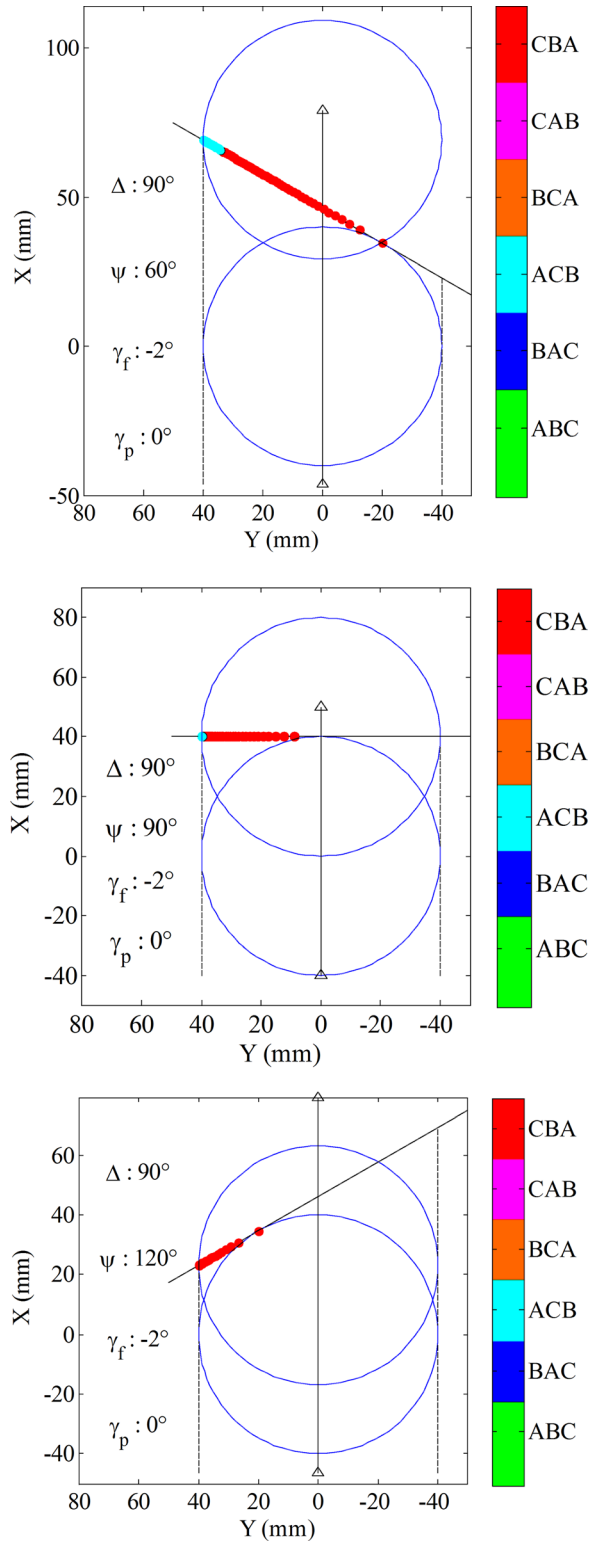**Fig. 12 Effects and interactions of parameters on burr height**

Fig. 13 EOS during tool exit path for three simulations $\Psi \in$ {60 deg, 90 deg, 120 deg}
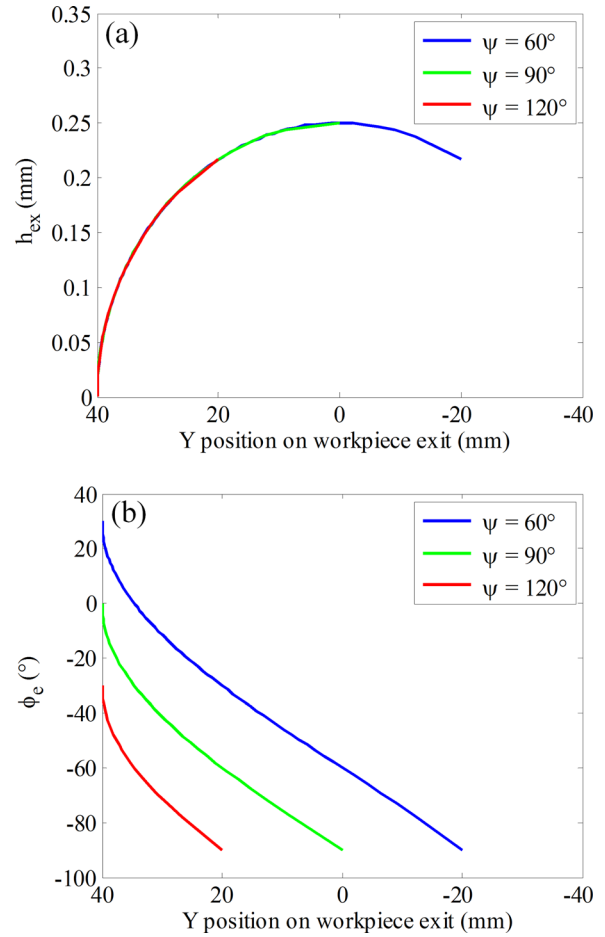

Fig. 14 Uncut chip thickness at the cutting edge exit h_{ex} (**a**) and cutting edge exit angle ϕ_e (**b**) during the three simulations $\Psi \in$ {60 deg, 90 deg, 120 deg}: $f_z = 0.25$ mm.rev^{-1}.th^{-1} and $a_e = D$

boundary length of cutting edge exit region is. The rest is generated during teeth entry, thus with no burr formation.

Figure 14 shows the important variation in h_{ex} and ϕ_e parameters along the part boundary. As long as the exit angle ϕ_e increases, the uncut chip thickness h_{ex} increases on the left milling side. It should be noted that there exists a significant interaction of these parameters with respect to burr height.
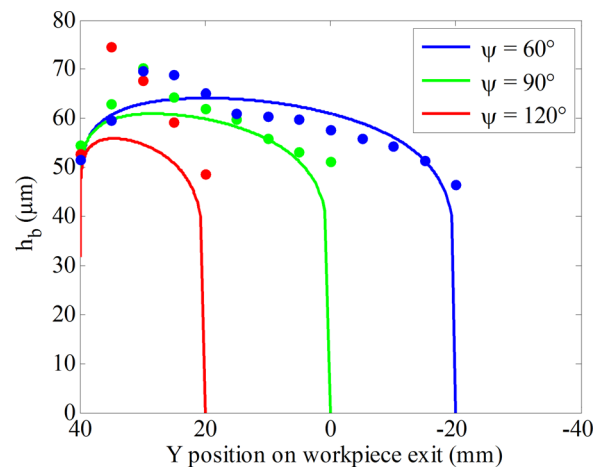

Fig. 15 Variation in burr height along workpiece boundary: experimental (points) versus simulations (curves): $\Psi \in$ {60 deg, 90 deg, 120 deg}, $V_c = 2500$ m/min, $f_z = 0.25$ mm.rev^{-1}.th^{-1}, $a_p = 2$ mm, $a_e = D$, and $\Delta = 90$ deg

value for the radial depth. The wedge angle is set at 90 deg, and the axial depth is fixed.

Figure 13 presents the different milling configurations and the corresponding EOS. For a 60 deg workpiece edge orientation, the part boundary is generated over a small range with an ACB EOS. For the two other cases, the sequence is CBA, which is the less favorable because it increases burr formation [18]. Nevertheless, the higher the workpiece edge orientation Ψ is, the lower the

Figure 15 presents the burr height values along the part boundary for the three simulations as well as those resulting from experiments. There is no burr generated during the tool teeth entry, and its height variation along the exit regions depends only on the h_{ex} and ϕ_e interaction, the workpiece wedge angle, and the axial depth of cut being constant.

The simulated burr heights fit quite well with the experimental ones, even if there is a small magnitude error. This can be explained by the use of different cutting inserts for local model calibration compared to the three applications. The highest gap between simulation and experimentation is obtained with a workpiece edge orientation Ψ equal to deg.

During the tool exit, for the three simulations, the uncut chip thickness on the tool's left side is the lowest h_{ex}, which tends to reduce burr formation. However, if the exit angle ϕ_e becomes close to zero, flow direction is nearly normal to the workpiece boundary, which leads to an increase in burr formation. On the tool's right side, when there is no teeth exit, i.e., no burr, the situation is the opposite: thickness h_{ex} is high, but angle ϕ_e is close to 90 deg. Because of these opposite tendencies for major influential parameters, the maximum burr height value appears along the part boundary. These trends are confirmed by the experimental results.

From the comparison of application cases, it globally appears that the use of a tool path direction with a higher workpiece edge orientation Ψ leads to a decrease in the length of the part boundary where the burr is generated.

Therefore, a maximum radial depth of cut of 20 mm, 40 mm, and 60 mm for a workpiece edge orientation Ψ of 60 deg, 90 deg, and 120 deg, respectively, enables a drastic reduction in burr size, especially when entry burrs are really trivial. This would be the easiest solution to integrate into tool path programing. Indirectly, this is the path strategy to avoid teeth exit, or to change the EOS, as proposed in Ref. [19]. Nevertheless, the complexity of the tool path trajectory results from the openwork part geometry and the application is not obvious.

5 Conclusions

This article presents both an experimental study and a predictive model of burr formation during plane milling. A local approach is developed to take into account significant parameters linked to the cutting conditions, including 3D cutting specific aspects of milling. There is a special consideration for the workpiece wedge angle, which has not been studied until now. Parameter interactions are studied, and it is demonstrated that the interaction of the uncut chip thickness at the cutting edge exit h_{ex} with the cutting edge exit angle ϕ_e is the most important one.

A full geometrical parameterization is proposed to deal with most face-milling operations during tool exits and entries. Based on this parameterization, a useful model is provided allowing to predict burr height in any region along openwork part boundaries even if local parameters are changing. The methodology has been experimentally validated. It is a quantitative approach, which is complementary to the qualitative EOS one and can be integrated into the milling strategy in order to reduce burrs and contribute to the design process and the evaluation of the possible need for deburring operations. Furthermore, it is presently established that the EOS ranking versus burr height can be affected by the workpiece wedge angle.

Complementary investigations will focus on the effect of tool wear and on the fundamentals of burr formation to explain phenomena like the variation in lateral burr height.
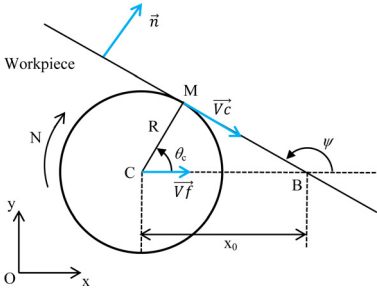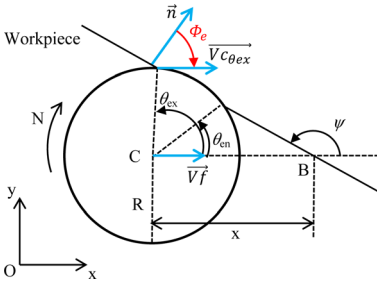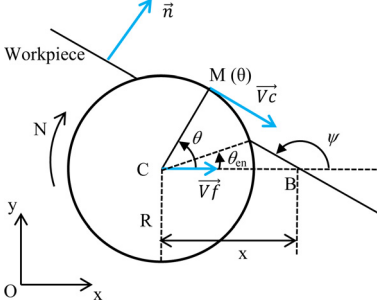
Acknowledgment
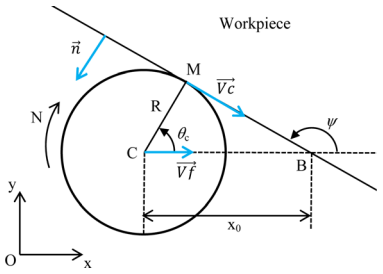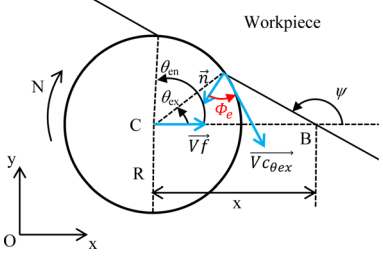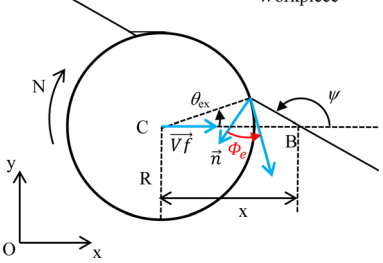
Appendix A: Geometrical Parameters During Cylindrical Milling

Tool path parallel to the workpiece edge	θ_{ex}	θ_{en}	h_{ex}	h_{en}	Φ_e
Up end milling	$\arcsin\left(\dfrac{R-a_e}{R}\right)$	—	$R+f_z\cdot\sin\left(\dfrac{\pi}{2}-\theta_{ex}\right)$ $-\sqrt{R^2-\left(f_z\cdot\cos\left(\dfrac{\pi}{2}-\theta_{ex}\right)\right)^2}$	—	θ_{ex}
Down end milling	—	$-\arcsin\left(\dfrac{R-a_e}{R}\right)$	—	$R+f_z\cdot\sin\left(\dfrac{\pi}{2}+\theta_{en}\right)$ $-\sqrt{R^2-\left(f_z\cdot\cos\left(\dfrac{\pi}{2}+\theta_{en}\right)\right)^2}$	—
Face milling	$-\arcsin\left(\dfrac{a_e+e}{2*R}\right)$	$\arcsin\left(\dfrac{a_e+e}{2*R}\right)$	$R+f_z\cdot\sin\left(\dfrac{\pi}{2}-\theta_{ex}\right)$ $-\sqrt{R^2-\left(f_z\cdot\cos\left(\dfrac{\pi}{2}-\theta_{ex}\right)\right)^2}$	$R+f_z\cdot\sin\left(\dfrac{\pi}{2}+\theta_{en}\right)$ $-\sqrt{R^2-\left(f_z\cdot\cos\left(\dfrac{\pi}{2}+\theta_{en}\right)\right)^2}$	θ_{ex}

Appendix B: Geometrical Parameters During Cylindrical Tool Exit

Tool path exit	θ_{ex}	θ_{en}	h_{ex}	h_{en}	Φ_e
First step	If $\psi > 90\,\mathrm{deg}\ :\ \theta_c = \arccos(\sin(\psi))$ If $\psi < 90\,\mathrm{deg}\ :\ \theta_c = -\arccos(\sin(\psi))$	—	—	—	—
Second step	$\theta_c + \arccos\left(\dfrac{R - (x - x_0)\sin(\psi)}{R}\right)$	$\theta_c - \arccos\left(\dfrac{R - (x - x_0)\sin(\psi)}{R}\right)$	$R + f_z \cdot \sin\left(\dfrac{\pi}{2} - \theta_{\mathrm{ex}}\right)$ $-\sqrt{R^2 - \left(f_z \cdot \cos\left(\dfrac{\pi}{2} - \theta_{\mathrm{ex}}\right)\right)^2}$	$R + f_z \cdot \sin\left(\dfrac{\pi}{2} + \theta_{\mathrm{en}}\right)$ $-\sqrt{R^2 - \left(f_z \cdot \cos\left(\dfrac{\pi}{2} + \theta_{\mathrm{en}}\right)\right)^2}$	$\theta_{\mathrm{ex}} - \psi$
Third step	—	$\theta_c - \arccos\left(\dfrac{R - (x - x_0)\sin(\psi)}{R}\right)$	—	$R + f_z \cdot \sin\left(\dfrac{\pi}{2} + \theta_{\mathrm{en}}\right)$ $-\sqrt{R^2 - \left(f_z \cdot \cos\left(\dfrac{\pi}{2} + \theta_{\mathrm{en}}\right)\right)^2}$	—

Appendix C: Geometrical Parameters During Cylindrical Tool Entrance

Tool path entrance		θ_{ex}	θ_{en}	h_{ex}	h_{en}	Φ_e
First step		If $\psi > 90\deg\ :\ \theta_c = \arccos(\sin(\psi))$ If $\psi < 90\deg\ :\ \theta_c = -\arccos(\sin(\psi))$	—	—	—	—
Second step		$\theta_c - \arccos\left(\dfrac{R - (x - x_0)\sin(\psi)}{R}\right)$	$\theta_c + \arccos\left(\dfrac{R - (x - x_0)\sin(\psi)}{R}\right)$	$R + f_z \cdot \sin\left(\dfrac{\pi}{2} + \theta_{\text{ex}}\right)$ $-\sqrt{R^2 - \left(f_z \cdot \cos\left(\dfrac{\pi}{2} + \theta_{\text{ex}}\right)\right)^2}$	$R + f_z \cdot \sin\left(\dfrac{\pi}{2} - \theta_{\text{en}}\right)$ $-\sqrt{R^2 - \left(f_z \cdot \cos\left(\frac{\pi}{2} - \theta_{\text{en}}\right)\right)^2}$	$\theta_{\text{ex}} - \psi + \pi$
Third step		$\theta_c - \arccos\left(\dfrac{R - (x - x_0)\sin(\psi)}{R}\right)$	—	$R + f_z \cdot \sin\left(\dfrac{\pi}{2} + \theta_{\text{ex}}\right)$ $-\sqrt{R^2 - \left(f_z \cdot \cos\left(\dfrac{\pi}{2} + \theta_{\text{ex}}\right)\right)^2}$	—	$\theta_{\text{ex}} - \psi + \pi$

Nomenclature

a_e = radial depth of cut
a_p = axial depth of cut
ave = average
D = tool diameter
EOS = exit order sequence
f_z = feed per tooth
h_b = burr height
$h_{b\ \text{ave}}$ = average burr height
$h_{b\ \text{max}}$ = maximum burr height
h_{en} = uncut chip thickness at the cutting edge entry
h_{ex} = uncut chip thickness at the cutting edge exit
max = maximum
$\mathbf{n}$ = normal vector
R = tool radius
V_c = cutting speed
Δ = workpiece wedge angle
θ_c = cutting edge contact position angle (contact with the workpiece boundary)
θ_{en} = entry position angle of the cutting edge
θ_{ex} = exit position angle of the cutting edge
Φ_e = cutting edge exit angle
Ψ = workpiece edge orientation

References

[1] Aurich, J. C., Dornfeld, D. A., Arrazola, P. J., Franke, V., Leitz, L., and Min, S., 2009, "Burrs: Analysis, Control and Removal," CIRP Ann. Manuf. Technol., **58**(2), pp. 519–542.
[2] Gillespie, L. K., and Blotter, P. T., 1976, "The Formation and Properties of Machining Burrs," ASME J. Eng. Ind., **98**(1), pp. 66–74.
[3] Hashimura, M., Hassamontr, J., and Dornfeld, D. A., 1999, "Effect of In-Plane Exit Angle and Rake Angles on Burr Height and Thickness in Face Milling Operation," ASME J. Manuf. Sci. Eng., **121**(1), pp. 13–19.
[4] Preś, P., Skoczyński, W., and Jaśkiewicz, K., 2014, "Research and Modeling Workpiece Edge Formation Process During Orthogonal Cutting," Archiv. Civil Mech. Eng., **14**(4), pp. 622–635.
[5] Ko, S. L., and Dornfeld, D. A., 1991, "A Study on Burr Formation Mechanism," ASME J. Eng. Mater. Technol., **113**(1), pp. 75–87.
[6] Park, I. W., and Dornfeld, D. A., 2000, "A Study of Burr Formation Processes Using the Finite Element Method: Part I," ASME J. Eng. Mater. Technol., **122**(2), pp. 221–228.
[7] Park, I. W., and Dornfeld, D. A., 2000, "A Study of Burr Formation Processes Using the Finite Element Method: Part II—The Influences of Exit Angle, Rake Angle, and Backup Material on Burr Formation Processes," ASME J. Eng. Mater. Technol., **122**(2), pp. 229–237.
[8] Sartkulvanicha, P., Sahlana, H., and Altana, T., 2007, "A Finite Element Analysis of Burr Formation in Face Milling of a Cast Aluminum Alloy," Mach. Sci. Technol., **11**(2), pp. 157–181.
[9] Niknam, S. A., and Songmene, V., 2014, "Analytical Modeling of Slot Milling Exit Burr Size," Int. J. Adv. Manuf. Technol., **73**(1), pp. 421–432.
[10] Niknam, S. A., and Songmene, V., 2013, "Modeling of Burr Thickness in Milling of Ductile Materials," Int. J. Adv. Manuf. Technol., **66**(9), pp. 2029–2039.
[11] Jones, S. D., and Furness, R. J., 1997, "An Experimental Study of Burr Formation for Face Milling 356 Aluminium," Trans. NAMRI/SME, **25**, pp. 183–188.
[12] Chern, G. L., 2006, "Experimental Observation and Analysis of Burr Formation Mechanisms in Face Milling of Aluminum Alloys," Int. J. Mach. Tools Manuf., **46**(12–13), pp. 1517–1525.
[13] Lin, R. T., 2000, "Experimental Study of Burr Formation and Tool Chipping in the Face Milling of Stainless Steel," J. Mater. Process. Technol., **108**(1), pp. 12–20.
[14] Da Silva, L. C., Da Mota, P. R., Da Silva, M. B., Ezugwu, E. O., and Machado, A. R., 2015, "Study of Burr Behavior in Face Milling of PH 13-8 Mo Stainless Steel," CIRP J. Manuf. Sci. Technol., **8**, pp. 34–42.
[15] Olvera, O., and Barrow, G., 1996, "An Experimental Study of Burr Formation in Square Shoulder Face Milling," Int. J. Mach. Tools Manuf., **36**(9), pp. 1005–1020.
[16] Olvera, O., and Barrow, G., 1998, "Influence of Exist Angle and Tool Nose Geometry on Burr Formation in Face Milling Operations," Proc. Inst. Mech. Eng., Part B, **212**(1), pp. 59–72.
[17] Da Silva, L. C., De Melo, A. C. A., Machado, A. R., Da Silva, M. B., and Souza Júnior, A. M., 2006, "Application of Factorial Design for Studying the Burr Behaviour During Face Milling of Motor Engine Blocks," J. Mater. Process. Technol., **179**(1–3), pp. 154–160.
[18] Kumar, S., and Dornfeld, D. A., 2003, "Basic Approach to a Prediction System for Burr Formation in Face Milling," J. Manuf. Process., **5**(2), pp. 127–142.
[19] Chu, C. H., and Dornfeld, D. A., 2005, "Geometric Approaches for Reducing Burr Formation in Planar Milling by Avoiding Tool Exits," J. Manuf. Process., **7**(2), pp. 182–195.
[20] ISO 13715, Technical Drawings—Edges of Undefined Shape—Vocabulary and Indications, International Organization for Standardization.